

High-density carbon capsule experiments on the national ignition facility

J. S. Ross, D. Ho, J. Milovich, T. Döppner, J. McNaney, A. G. MacPhee, A. Hamza, J. Biener, H. F. Robey, E. L. Dewald, R. Tommasini, L. Divol, S. Le Pape, L. Berzak Hopkins, P. M. Celliers, O. Landen, N. B. Meezan, and A. J. Mackinnon

Lawrence Livermore National Laboratory, P.O. Box 808, Livermore, California 94551, USA

(Received 2 January 2014; published 25 February 2015)

Indirect-drive implosions with a high-density carbon (HDC) capsule were conducted on the National Ignition Facility (NIF) to test HDC properties as an ablator material for inertial confinement fusion. A series of five experiments were completed with 76- μm -thick HDC capsules using a four-shock laser pulse optimized for HDC. The pulse delivered a total energy of 1.3 MJ with a peak power of 360 TW. The experiment demonstrated good laser to target coupling ($\sim 90\%$) and excellent nuclear performance. A deuterium and tritium gas-filled HDC capsule implosion produced a neutron yield of $1.6 \times 10^{15} \pm 3 \times 10^{13}$, a yield over simulated in one dimension of 70%.

DOI: [10.1103/PhysRevE.91.021101](https://doi.org/10.1103/PhysRevE.91.021101)

PACS number(s): 52.57.Bc, 52.50.Jm, 52.57.Fg

The goal of indirect-drive inertial confinement fusion (ICF) is to uniformly compress a fuel capsule with x-ray radiation to a density and temperature where thermonuclear fusion burns an appreciable fraction ($\geq 1/3$) of the total deuterium and tritium (DT) fuel mixture. The x-ray drive is generated by the deposition of laser energy in a gold hohlraum with the fuel capsule positioned at the hohlraum center. The capsule ablator, surrounding the DT ice and gas fuel, is burned off, or ablated, by the x-ray drive creating immense pressures at stagnation—on the order of 300 Gbar for ignition. The ablator material used so far on larger laser facilities has almost exclusively been silicon or germanium doped plastic (CH) [1–6]. Alternate ablator materials are an active area of research for ICF [7–9]. One possible alternative to CH is high-density carbon (HDC) [10,11]. HDC is nanocrystalline diamond and has a number of advantages over CH. HDC has a higher density than CH, and for the same initial outer diameter, results in a thinner initial shell and a larger initial inner diameter. This leads to an increase in mechanical (pdV) work on the larger fuel and hot spot volume. The thinner shell also leads to less absolute inward motion during shock compression, which produces an ablation front at larger radius when the peak of the drive and acceleration begins. This larger radius and therefore larger ablation surface area results in higher efficiency and more absorbed energy compared to CH. This allows HDC designs to reach ignition with a higher adiabat (the ratio of fuel pressure to the Fermi degenerate pressure) compared to CH ignition designs or to achieve higher gains for a similar adiabat. The larger initial inner radius also leads to an increase in fuel and hot spot mass for the same initial fill density. HDC can also be polished to a much higher surface quality than CH ($\sim 10\times$ improvement) due to its nanocrystalline nature [11]. There are possible disadvantages as well. Changing the capsule material may cause an increase in backscatter [12] as the ablator fills the hohlraum, solid or partial melting of the HDC during compression may provide microstructures that seed hydrodynamic instability growth [8,13,14], and reduced ablation front scale lengths could produce larger overall instability growth leading to ablator mix into the hot spot.

We present measurements of HDC capsule implosion performance on the National Ignition Facility [15] at ICF drive conditions. A five-shot campaign was completed using HDC capsules in three different target platforms. Two “keyhole”

targets [16] were fielded, the first with a truncated laser pulse for an initial assessment of backscatter and hohlraum performance. Hohlraum drive and laser plasma instability losses were similar to experiments using a CH ablator in a gas-filled hohlraum [17,18]. A small improvement in inner beam propagation was observed, likely due to the slightly smaller initial outer diameter of the HDC capsules (the capsules fielded on these experiments had an inner radius 70 μm larger and an outer radius 40 μm smaller than typical CH capsules). The second “keyhole” was used to measure shock velocities and shock timing. No indications of partial melting or refreeze were observed in the shock timing data. Two one-dimensional (1D) convergent ablator targets [19] were fielded to measure the in-flight capsule velocity and hot spot shape. The final shot in the campaign was a cryogenic symcap target [1] filled with DT gas to assess nuclear performance. The target produced a yield of $1.6 \times 10^{15} \pm 3 \times 10^{13}$, a yield over 1D simulated of 70% in a nonlayered target on the National Ignition Facility (NIF). This implosion performance indicates that ablator mix into the hot spot is minimal. These experiments confirm HDC as a viable ablator material for ICF and open the path for higher velocity layered implosions.

All of the experiments in this campaign use a gold hohlraum and capsule configuration as shown in Fig. 1. The spherical HDC capsules are $76 \pm 1.0 \mu\text{m}$ in thickness with an inner radius of $1000 \pm 2 \mu\text{m}$. The HDC is nanocrystalline: the grain size is of the order of nanometers, with an average density of 3.32 g/cc. The capsules are located at the center of gold hohlraums, which measure 9.425 mm in length and 5.75 mm in diameter. The hohlraums have laser entrance holes 3.10 mm in diameter and are filled with 1.2 mg/cc of helium. The targets are fielded at a temperature of 32 K to reduce the helium gas-fill pressure on the hohlraum windows. The exception is the “keyhole” targets which use a liquid deuterium capsule fill and were therefore fielded at 21.5 K [16].

The laser pulse shape is shown in Fig. 2 and compared with typical CH pulse shapes. A peak power of 360 TW with a total laser energy of 1.3 MJ is delivered by 192 laser beams at a wavelength of 351 nm (3ω). The HDC pulse is significantly shorter than the two CH pulses due to the reduced capsule thickness for HDC to maintain a similar capsule mass and the HDC pulse has a slightly stronger first shock strength to ensure at least partial melting of the HDC. The time between the

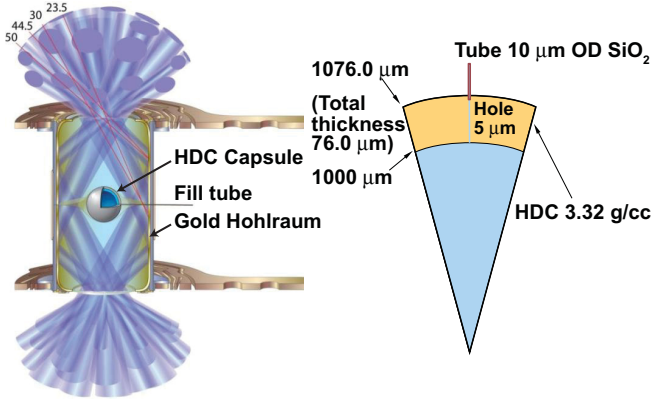


FIG. 1. (Color online) The target configuration is shown. The hohlraum is 9.425 mm in length and 5.75 mm in diameter. The 192 laser beams enter the hohlraum through two laser entrance holes 3.101 mm in diameter. The high-density carbon capsule is located at the center of the hohlraum and has a shell thickness of 76 μm .

second, third, and fourth rises of the laser pulse are increased for the “keyhole” targets to allow accurate measurements of the individual shocks [16]; the pulse is also truncated early. Eight laser beams are removed from the hohlraum and used to drive an x-ray backlighter target for the 1D convergent ablator experiments [19]. A subset of the remaining beams is run at a higher power and energy to compensate for the missing energy during these experiments.

Figure 3(a) shows the VISAR [20] streaked interferometer data from the keyhole experiment. Time runs from left to right with vertical motion of the fringes being directly proportional to the shock velocity. Upward fringe motion is an indication of an accelerating shock. A mirror is located near the center of the HDC capsule to reflect a portion of the VISAR laser beam toward the pole [21]. This allows a simultaneous measurement of the shock trajectory along the equator and pole directions. Discontinuities in the fringe position indicate the break out of a shock from one material to another (labeled “1”) or the arrival of an overtaking shock (labeled “2,” “3,” and “4”). The first shock level in the shell is at a pressure of 600 GPa,

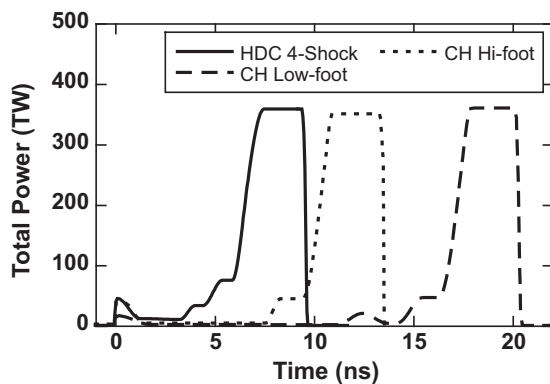


FIG. 2. The laser pulse shape for the HDC capsule (solid line) is compared to the high-foot CH pulse shape (dotted line) and the low-foot CH pulse (dashed line). All three laser pulses have a total energy of 1.3 MJ and powers between 350 and 360 TW.

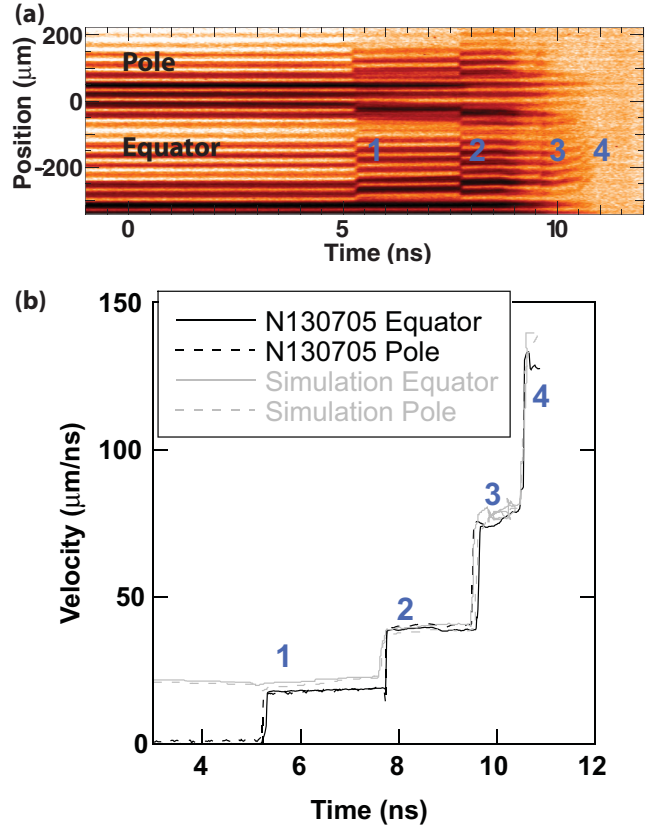


FIG. 3. (Color online) (a) VISAR streaked interferometry image with the shock breakout from the HDC ablator into the liquid deuterium and shock mergers 2, 3, and 4 are shown. (b) The measured shock velocity (black lines) compared to simulations (gray lines) is shown for the pole and equator views. Due to the opacity of the HDC, VISAR is unable to measure the velocity of the shock until it breaks out of the ablator at 5.2 ns.

which is within the liquid coexistence region [22], where the shock front is known to be smooth [23]. This is confirmed by the smooth breakout pattern of the first shock in the VISAR record. The measured velocity of the leading shock is shown in Fig. 3(b) and compared to postshot simulations. The simulations accurately reproduce the measured velocities and shock merger times using drive multipliers [24] similar to those used for CH implosions, giving us confidence that the carbon equation of state [25] and hohlraum modeling are adequate to assess and minimize the adiabat of HDC capsule implosions using the methodology described by Robey *et al.* [16]. The timing and depth of the shock mergers are adjusted to simultaneously merge just inside the fuel layer, which minimizes the adiabat and allows for maximum compression of the DT fuel.

A three color laser configuration was used to control capsule shape via crossed-beam energy transfer (CBET) [26]. For the first shot a wavelength difference of 2.83 \AA between the 23.5° beams and the outer beams and 2.43 \AA between the 30° beams and the outer beams was used. The equatorial hot spot shape at capsule stagnation is quantified by decomposing the x-ray flux asymmetry into Legendre polynomials [27,28], P_n . Odd orders ($n = 1, 3, \text{etc.}$) are minimal due to up-down

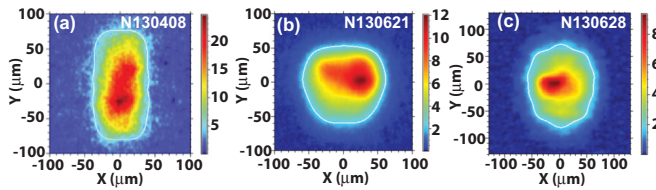


FIG. 4. (Color online) The time integrated x-ray emission from the hot spot is shown for the two deuterium-filled ConA experiments and the DT-filled symcap experiment. (a) With a wavelength separation of $+2.83 \text{ \AA} (+2.43 \text{ \AA})$ between the $30^\circ (23^\circ)$ beams and the outer beams, a prolate core image was observed. (b) After reducing the wavelength separation between the cones to $+1.73 \text{ \AA}$ and $+1.33 \text{ \AA}$, respectively, a nearly round core was produced. (c) This wavelength separation was then used for the DT symcap experiment producing a slightly prolate core.

symmetry. Low-order even modes ($n = 2, 4$) are critical to performance and controllable via modifications to the target geometry, laser pointing, and laser cone fraction changes through CBET. The x-ray emission from the core was prolate ($P_2/P_0 = 0.55$) at the wavelengths of 2.83 and 2.43 \AA [Fig. 4(a)], an indication that the capsule was overdriven on the equator. To correct this asymmetry the wavelength separation between cones was reduced to 1.73 and 1.33 \AA , respectively, resulting in a nearly round x-ray core image [Fig. 4(b)] with a $P_2/P_0 = 0.0 \pm 0.01$. This wavelength change had the additional benefit of increasing laser to target coupling from $86 \pm 2\%$ to $91 \pm 2\%$. The laser to target coupling is 100% minus the percentage of laser energy measured by the NIF backscattered diagnostics [29]. This improved coupling was primarily due to a decrease in inner beam stimulated Raman scattering. The hohlraum radiation temperature measured by Dante [30] was $293 \pm 5 \text{ eV}$ with an M -band fraction (percentage of the flux $> 1.8 \text{ keV}$) of $16\% \pm 1\%$.

Figure 5 shows the x-ray streaked radiograph of inflight HDC capsule ablaters. An iron backlighter foil is used to produce 6.7 keV x rays to backlight the imploding capsule. The time resolved x-ray image is shown in Fig. 5(a). The x-ray backlighter and diagnostic pointing were offset from the capsule center by $250 \mu\text{m}$ to center the field of view on

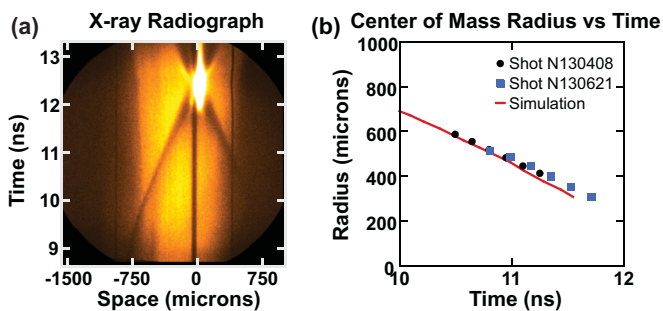


FIG. 5. (Color online) (a) The x-ray radiograph of the imploding HDC capsule is shown for shot N130621. Late in time the capsule self-emission dominates the recorded signal. (b) The measured center of mass radius for shots N130408 (black circles) and N130621 (blue squares) is compared to a postshot simulation (red line) using drive multipliers to match the measured bang time.

half of the capsule and increase the range of radii recorded. The x-ray radiography measures the in-flight capsule shell from 10.6 ns until 11.7 ns; this equates to a capsule radius of $550\text{--}320 \mu\text{m}$. The velocity of the center of mass reaches a maximum value of $265 \pm 3 \mu\text{m}$ at the end of the recorded trajectory, corresponding to a radius of $\sim 320 \mu\text{m}$. The center of mass velocity is in close agreement with simulations until the capsule reaches a radius of $500 \mu\text{m}$ at which point a discrepancy begins to develop. This is most likely due to a decompression of the capsule [31], which the model does not accurately reproduce during the coating phase (the drive lasers have been off for more than 1 ns) of the implosion.

The final shot in this campaign was a DT gas-filled cryogenic capsule implosion, shot number N130628. The capsule was filled with 8.1 mg/cc of DT gas. The DT neutron yield produced was $1.6 \times 10^{15} \pm 3 \times 10^{13}$ with an ion temperature of $2.9 \pm 0.1 \text{ keV}$. The NIF neutron imaging system [32] was used to image the primary neutrons. An average radius, $P_0 = 57 \pm 4 \mu\text{m}$ with a $P_2/P_0 = 0.19 \pm 0.08$ was measured from the imploded core. The time integrated x-ray emission from the core was also measured; the average radius was $P_0 = 65 \pm 4 \mu\text{m}$ with a $P_2/P_0 = 0.14 \pm 0.03$, very similar to the neutron shape. The nuclear burn width was 340 ps. Using these measured quantities and a 1D hot spot model [33] the hot spot stagnation pressure is inferred to be 32.5 Gbar, the internal energy is 5.8 kJ, and the mass is $20 \mu\text{g}$. These values are in close agreement with postshot simulations.

The HDC capsule performance was close to expectations based on 1D simulations outperforming similar shots using a CH ablator. Detailed postshot simulations using the radiation hydrodynamics code HYDRA [34] were completed using the methodology described by Jones *et al.* [24] where the incident laser energy is adjusted to match the measured shock timing from the keyhole experiment, the in-flight center of mass radius from the ConA experiment, and the time of peak capsule x-ray emission from the DT gas-fill experiment. To match these measurements a multiplier on the peak drive of 0.72 ± 0.02 is required. This is similar to the multiplier of 0.75 ± 0.02 [35] used for four-shock CH experiments [36]. The 1D simulated yield was calculated to be 2.28×10^{15} resulting in a yield over 1D simulated (YoS) of 70%. The measured ion temperature, $2.9 \pm 0.1 \text{ keV}$ also matches the temperature 2.92 keV predicted by simulations. The simulations described above are “clean” and do not attempt to resolve the Rayleigh-Taylor instability or to include ablator mix into the hot spot.

The measured HDC yield is compared to the 1D simulated yield in Fig. 6. A range of CH implosions is also shown with convergence ratios ranging from 5 to 40. The HDC experiment produced twice the yield of previous CH gas-filled symcaps with a similar convergence ratio. This is consistent with expectations. The increase in DT fuel due to the increased capsule volume should increase the yield by $\sim 30\%$ based on simulations. The capsule fill densities were slightly different for the CH symcaps ranging from 8.6 mg/cc to 9.7 mg/cc. The HDC capsules are predicted to absorb 50% more energy as well, which equates to an increased yield of $\sim 65\%$ based on 1D simulations. This is a very encouraging result and confirmation that HDC is a viable capsule material for ICF implosions. The HDC capsules also have a number of advantages that are not fully captured in postshot simulations and are likely to be

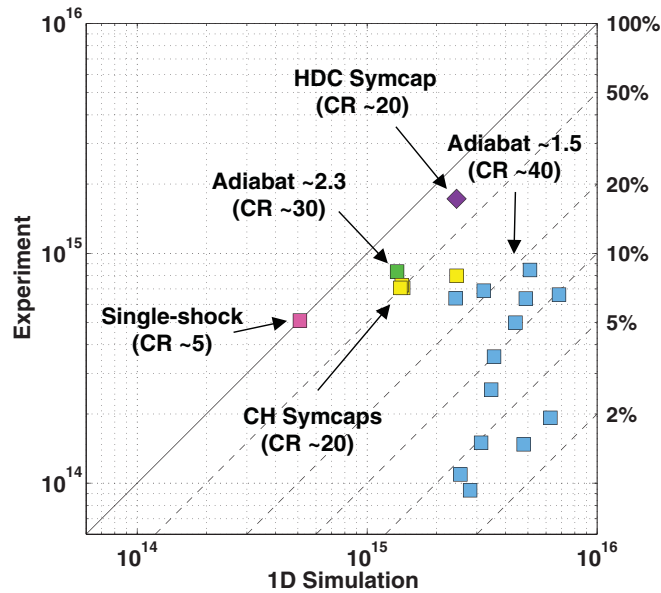


FIG. 6. (Color online) The measured experimental yield is compared to the 1D simulated yield for a collection of NIF experiments (DT and Symcap shots between N111103 and N130812) with different convergence ratios (CR). The HDC DT symcap experiment (purple diamond) is close to 1D performance with a yield over simulated of 70%. The remaining points are CH capsule experiments with DT ice layers using the high-foot pulse [37] (green square, CR ~ 30) and low-foot pulse [38] (blue squares, CR ~ 40), low-foot DT symcaps (yellow squares, CR ~ 20) and an exploding pusher [39] (pink square, CR ~ 5). The typical convergence ratio for each experiment type is shown ranging from 5 for the exploding pusher to 40 for the layered DT shots.

important when trying to achieve higher convergence ratios. Improved surface finishes are predicted to reduce instability growth and reduced mix. The HDC capsules are also undoped, which causes reduced ablation front instability growth. Upcoming experiments are planned to quantify these effects.

Hydrogrowth radiography experiments [40] will investigate the instability growth on the capsule surface, and direct comparison experiments using tungsten-doped HDC and undoped CH are planned to isolate the effect of dopants.

Future experiments are also planned to test HDC capsules in near-vacuum hohlraums. Near-vacuum hohlraums have significant advantages over the typical gas-filled hohlraum. They have minimal backscatter: near 2% compared to 10%–15% for a gas-filled hohlraum, and drive multipliers are not required to match observables in postshot simulations. These two advantages result in an increased drive of 30%–40%. There is also minimal crossed-beam energy transfer in a near-vacuum hohlraum, simplifying control of drive symmetry. The major disadvantage of near-vacuum hohlraums is increased wall motion and Au bubble expansion, leading to impaired propagation of the inner beams. Hence near-vacuum hohlraums are less attractive for CH capsule implosions requiring a laser pulse duration of 15 ns or longer (see Fig. 2), but are candidates at current scales for an HDC ablator implosion which uses a comparably shorter drive pulse length. We are hoping to push a near-vacuum hohlraum with an HDC capsule into the α heating regime (where α particle deposition significantly enhances the neutron yield production) in upcoming experiments.

In conclusion, we have performed implosion experiments using HDC capsules on the NIF with laser pulse energies of 1.3 MJ and peak power reaching 360 TW. A neutron yield in excess of 1.6×10^{15} was achieved with a gas-filled DT symcap approximately $2\times$ higher than similarly filled CH ablator capsules. These experiments confirm HDC as a viable material for ICF implosions. Future experiments are planned with HDC capsules with the goal to reach the α heating regime and eventually ignition.

This work was performed under the auspices of the U.S. Department of Energy by Lawrence Livermore National Laboratory under Contract No. DE-AC52-07NA27344 and was partially funded by the Laboratory Directed Research and Development Program under project tracking code 06-ERD-056.

- [1] S. H. Glenzer, B. J. MacGowan, N. B. Meezan, P. Adams, J. Alfonso, E. T. Alger, Z. Alherz, L. F. Alvarez, S. S. Alvarez, P. V. Amick *et al.*, *Phys. Rev. Lett.* **106**, 085004 (2011).
- [2] D. D. Meyerhofer, R. L. McCrory, R. Betti, T. R. Boehly, D. T. Casey, T. J. B. Collins, R. S. Craxton, J. A. Delettrez, D. H. Edgell, R. Epstein *et al.*, *Nucl. Fusion* **51**, 053010 (2011).
- [3] H. F. Robey, P. Amendt, H. S. Park, R. P. J. Town, J. L. Milovich, T. Doeppner, D. E. Hinkel, R. Wallace, C. Sorce, D. J. Strozzi *et al.*, *Phys. Plasmas* **17**, 056313 (2010).
- [4] J. L. Kline, D. A. Callahan, S. H. Glenzer, N. B. Meezan, J. D. Moody, D. E. Hinkel, O. S. Jones, A. J. Mackinnon, R. Benedetti, R. L. Berger *et al.*, *Phys. Plasmas* **20**, 056314 (2013).
- [5] J. S. Ross, P. Amendt, L. J. Atherton, M. Dunne, S. H. Glenzer, J. D. Lindl, D. Meeker, E. I. Moses, A. Nikroo, and R. Wallace, *Sci. Rep.* **3**, 1453 (2013).
- [6] R. McCrory, R. Bahr, R. Betti, T. Boehly, T. Collins, R. Craxton, J. Delettrez, W. Donaldson, R. Epstein, J. Frenje *et al.*, *Nucl. Fusion* **41**, 1413 (2001).
- [7] R. E. Olson, R. J. Leeper, A. Nobile, J. A. Oertel, G. A. Chandler, K. Cochrane, S. C. Dropinski, S. Evans, S. W. Haan, J. L. Kaae *et al.*, *Phys. Plasmas* **11**, 2778 (2004).
- [8] O. L. Landen, D. K. Bradley, D. G. Braun, V. A. Smalyuk, D. G. Hicks, P. M. Celliers, S. Prisbrey, R. Page, T. R. Boehly, S. W. Haan *et al.*, *J. Phys.: Conf. Ser.* **112**, 022004 (2008).
- [9] D. T. Michel, V. N. Goncharov, I. V. Igumenshchev, R. Epstein, and D. H. Froula, *Phys. Rev. Lett.* **111**, 245005 (2013).
- [10] M. Murakami and J. Meyer-ter Vehn, *Nucl. Fusion* **31**, 1315 (1991).
- [11] J. Biener, D. D. Ho, C. Wild, E. Woerner, M. M. Biener, B. S. El-dasher, D. G. Hicks, J. H. Eggert, P. M. Celliers, G. W. Collins *et al.*, *Nucl. Fusion* **49**, 112001 (2009).

- [12] P. Neumayer, R. L. Berger, D. Callahan, L. Divol, D. H. Froula, R. A. London, B. J. MacGowan, N. B. Meezan, P. A. Michel, J. S. Ross *et al.*, *Phys. Plasmas* **15**, 056307 (2008).
- [13] P. M. Celliers, D. J. Erskine, C. M. Sorce, D. G. Braun, O. L. Landen, and G. W. Collins, *Rev. Sci. Instrum.* **81**, 035101 (2010).
- [14] S. W. Haan, J. D. Lindl, D. A. Callahan, D. S. Clark, J. D. Salmonson, B. A. Hammel, L. J. Atherton, R. C. Cook, M. J. Edwards, S. Glenzer *et al.*, *Phys. Plasmas* **18**, 051001 (2011).
- [15] G. H. Miller, E. I. Moses, and C. R. Wuest, *Opt. Eng.* **43**, 2841 (2004).
- [16] H. F. Robey, T. R. Boehly, P. M. Celliers, J. H. Eggert, D. Hicks, R. F. Smith, R. Collins, M. W. Bowers, K. G. Krauter, P. S. Datte *et al.*, *Phys. Plasmas* **19**, 042706 (2012).
- [17] R. P. J. Town, M. D. Rosen, P. A. Michel, L. Divol, J. D. Moody, G. A. Kyrala, M. B. Schneider, J. L. Kline, C. A. Thomas, J. L. Milovich *et al.*, *Phys. Plasmas* **18**, 056302 (2011).
- [18] J. D. Moody, D. A. Callahan, D. E. Hinkel, P. A. Amendt, K. L. Baker, D. Bradley, P. M. Celliers, E. L. Dewald, L. Divol, T. Döppner *et al.*, *Phys. Plasmas* (1994–present) **21**, 056317 (2014).
- [19] D. G. Hicks, N. B. Meezan, E. L. Dewald, A. J. Mackinnon, R. E. Olson, D. A. Callahan, T. Döppner, L. R. Benedetti, D. K. Bradley, P. M. Celliers *et al.*, *Phys. Plasmas* **19**, 122702 (2012).
- [20] R. M. Malone, B. C. Frogget, M. I. Kaufman, T. W. Tunnell, R. L. Guyton, I. P. Reinbachs, P. W. Watts, J. R. Celeste, P. M. Celliers, T. L. Lee, B. J. MacGowan, E. W. Ng, R. B. Robinson, and L. G. Seppala, *Overview of the Line-Imaging VISAR Diagnostic at the National Ignition Facility (NIF)*, in *International Optical Design, Technical Digest (CD)* (Optical Society of America, Massachusetts, 2006), paper ThA5.
- [21] J. D. Moody, H. F. Robey, P. M. Celliers, D. H. Munro, D. A. Barker, K. L. Baker, T. Döppner, N. L. Hash, L. B. Hopkins, K. LaFortune *et al.*, *Phys. Plasmas* (1994–present) **21**, 092702 (2014).
- [22] J. H. Eggert, D. G. Hicks, P. M. Celliers, D. K. Bradley, R. S. McWilliams, R. Jeanloz, J. E. Miller, T. R. Boehly, and G. W. Collins, *Nat. Phys.* **6**, 40 (2009).
- [23] A. J. MacKinnon, N. Meezan, J. S. Ross, S. L. Pape, L. Berzak-Hopkins, L. Divol, J. M. D. Ho, A. Pak, T. D. J. Ralph, R. T. C. Thomas *et al.*, *Phys. Plasmas* **21**, 056318 (2014).
- [24] O. S. Jones, C. J. Cerjan, M. M. Marinak, J. L. Milovich, H. F. Robey, P. T. Springer, L. R. Benedetti, D. L. Bleuel, E. J. Bond, D. K. Bradley *et al.*, *Phys. Plasmas* **19**, 056315 (2012).
- [25] A. A. Correa, L. X. Benedict, D. A. Young, E. Schwegler, and S. A. Bonev, *Phys. Rev. B* **78**, 024101 (2008).
- [26] P. Michel, L. Divol, E. A. Williams, S. Weber, C. A. Thomas, D. A. Callahan, S. W. Haan, J. D. Salmonson, S. Dixit, D. E. Hinkel *et al.*, *Phys. Rev. Lett.* **102**, 025004 (2009).
- [27] A. A. Hauer, L. Suter, N. Delamater, D. Ress, L. Powers, G. Magelssen, D. Harris, O. Landen, E. Lindmann, W. Hsing *et al.*, *Phys. Plasmas* **2**, 2488 (1995).
- [28] O. L. Landen, P. A. Amendt, L. J. Suter, R. E. Turner, S. G. Glendinning, S. W. Haan, S. M. Pollaine, B. A. Hammel, M. Tabak, M. D. Rosen *et al.*, *Phys. Plasmas* **6**, 2137 (1999).
- [29] J. D. Moody, P. Datte, K. Krauter, E. Bond, P. A. Michel, S. H. Glenzer, L. Divol, C. Niemann, L. Suter, N. Meezan *et al.*, *Rev. Sci. Instrum.* **81**, 10D921 (2010).
- [30] E. Dewald, K. Campbell, R. Turner, O. Landen, S. Glenzer, M. Landon, and M. Rhodes, *Rev. Sci. Instrum.* **75**, 3759 (2004).
- [31] J. Lindl, O. Landen, J. Edwards, E. Moses, and NIC Team, *Phys. Plasmas* **21**, 020501 (2014).
- [32] M. D. Wilke, S. H. Batha, P. A. Bradley, R. D. Day, D. D. Clark, V. E. Fatherley, J. P. Finch, R. A. Gallegos, F. P. Garcia, G. P. Grim *et al.*, *Rev. Sci. Instrum.* **79**, 10E529 (2008).
- [33] C. Cerjan, P. T. Springer, and S. M. Sepke, *Phys. Plasmas* **20**, 056319 (2013).
- [34] M. M. Marinak, G. D. Kerbel, N. A. Gentile, O. Jones, D. Munro, S. Pollaine, T. R. Dittrich, and S. W. Haan, *Phys. Plasmas* **8**, 2275 (2001).
- [35] O. S. Jones (private communication).
- [36] This multiplier is consistent with previous publications [24, 19] after corrections to experimental inputs and simulation resolution are taken into account.
- [37] H. S. Park, O. A. Hurricane, D. A. Callahan, D. T. Casey, E. L. Dewald, T. R. Dittrich, T. Döppner, D. E. Hinkel, L. F. Berzak Hopkins, S. Le Pape *et al.*, *Phys. Rev. Lett.* **112**, 055001 (2014).
- [38] M. J. Edwards, P. K. Patel, J. D. Lindl, L. J. Atherton, S. H. Glenzer, S. W. Haan, J. D. Kilkenny, O. L. Landen, E. I. Moses, A. Nikroo *et al.*, *Phys. Plasmas* **20**, 070501 (2013).
- [39] S. Le Pape, L. Divol, L. Berzak Hopkins, A. Mackinnon, N. B. Meezan, D. Casey, J. Frenje, H. Herrmann, J. McNaney, T. Ma *et al.*, *Phys. Rev. Lett.* **112**, 225002 (2014).
- [40] V. A. Smalyuk, D. T. Casey, D. S. Clark, M. J. Edwards, S. W. Haan, A. Hamza, D. E. Hoover, W. W. Hsign, O. Hurricane, J. D. Kilkenny *et al.*, *Phys. Rev. Lett.* **112**, 185003 (2014).